EFFECT OF GAMMA RADIATION ON STEEL CORROSION

K. Daub, X. Zhang, J. Noel, D. Shoesmith, J.C. Wren

Department of Chemistry, the University of Western Ontario, London, Ontario

ABSTRACT

An important materials issue of nuclear reactors concerns the chemical effects of ionizing radiation on steel corrosion. The effect of radiation on the corrosion kinetics of carbon steel and stainless steel was studied by electrochemical and chemical speciation analyses. The changes in the steel corrosion behaviour during the exposure to gamma radiation were followed by corrosion potential and electrochemical impedance measurements. The corrosion kinetic measurements were also performed with steels exposed to H_2O_2 under non-irradiation conditions, and found the response of the corroding steel to gamma radiation at room temperature could be mimicked with chemical addition of H_2O_2 .

KEYWORDS

Corrosion kinetics, carbon steel, stainless steel, water radiolysis, gamma radiation, corrosion potential, passive oxide films

1. INTRODUCTION

A key component of the CANDU designed nuclear reactor is the heat transport system (HTS), which contains heavy water and carries the heat released from the reactor core to the steam generator along a temperature gradient. The HTS includes an array of zirconium alloy tubes in the reactor core that are connected to the coolant pumps and steam generators with feeder pipes made of carbon steel. Although feeder pipes are currently composed of carbon steel, AECL is considering using stainless steel with the newly designed ACR-1000 given stainless steel's exceptional corrosion resistance [1].

While carbon steel, and especially stainless steel, are very resistant to degradation through corrosion under the CANDU coolant chemistry conditions (pH \sim 10 controlled by LiOH addition and low corrosion potential controlled by H₂ addition), the steel will inevitably be exposed to water radiolysis products within the coolant (since the coolant passes through the high radiation field in the reactor core). Water can degrade under high-energy irradiation as follows [2]:

$$H_2O \rightarrow \bullet OH, e_{aq}^-, H_{\bullet}, HO_{2\bullet}, H_2, H_2O_2, H^+$$
 (1)

Where the primary radiolysis products further react to form secondary products such as O_2 and ${}^{\bullet}O_2^{-}$. It can be seen that a number of reactive oxidizing and reducing species are produced, all of which can affect the local oxidation potential of the coolant and corrosion of steel [3,4]. The concentration and rate of production of these species can determine the formation and degradation of any metal oxides and the oxidation states of metallic ions present in the material, for example, iron. A representation of the overall synergistic circuit is represented in Figure 1.

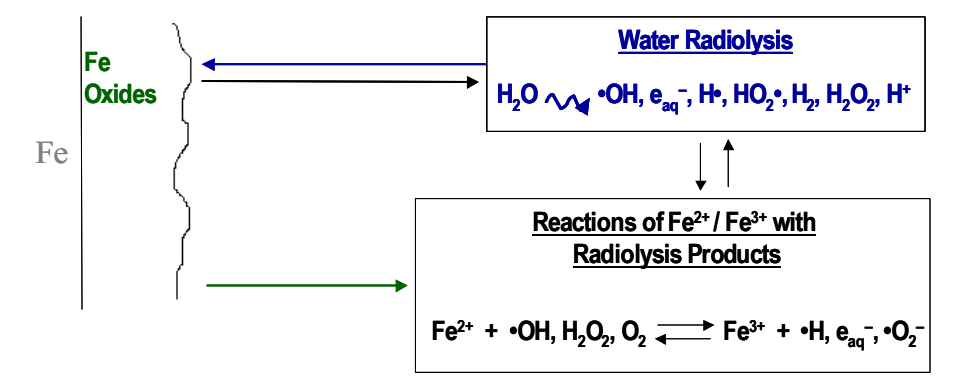


Figure 1: Synergistic Circuit of Steel, Soluble Fe²⁺, and Water Radiolysis Products.

The parameters affecting corrosion are temperature, pressure, pH, composition of the electrolyte, radiation dose, radiolysis products concentrations, and the morphology of the oxides formed on the steel. Our research is focused on the kinetics and mechanism of corrosion of various oxide films under controlled radiation doses at room temperature. Gas and aqueous samples of the system were analyzed for H₂, O₂, and H₂O₂, using a Gas Chromatography (GC) equipped with Mass Selective, Thermal Conductivity, and Electron Capture detectors (MSD/TCD/ECD) for O₂ and H₂ analysis and a UV-visible spectrophotometer for H₂O₂ analysis. Finally, electrochemical techniques were used to analyze the redox reactions involved in the formation of oxide films, and their reaction with radiolysis products.

2. EXPERIMENTAL

2.1 Electrochemical Setup

A three-electrode system, consisting of a working electrode (WE), a reference electrode (RE), and a counter electrode (CE) was used, Figure 2. The WE was composed of carbon steel or stainless steel 316L with a single flat exposed surface area, and the CE was a platinum mesh-wire. The RE was an Hg/HgO Electrode in 1.0 M KOH solution, which has shown to be more resistant to radiation than the saturated calomel electrode (SCE) or Ag/AgCl₂ electrode. The potential of the RE is 0.37 V versus the Standard Hydrogen Electrode (SHE). Although data was obtained using an Hg/HgO reference electrode, all potential values are quoted against SCE to facilitate comparison to other literature values. The potential of an Hg/HgO reference electrode against SCE is 0.13 V.

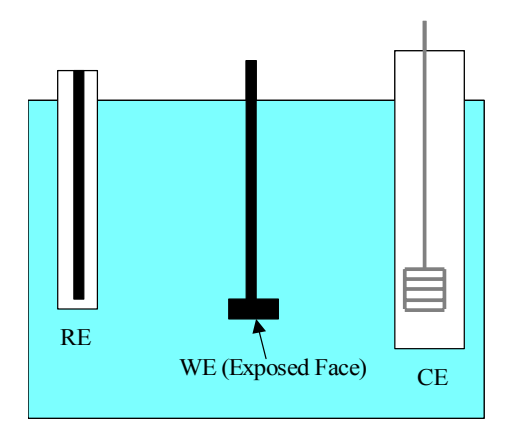


Figure 2: Schematic Layout of Three-electrode Cell, Containing a Working Electrode (WE), a Reference Electrode (RE), and a Counter Electrode (CE).

2.2 Working Electrodes

All experiments were performed using A516 Gr70 carbon steel and Austenitic grade 316L stainless steel. The composition of the carbon steel samples (by % weight) were 0.31 C, 1.0 Mn, 0.035 P. 0.04 S, 0.25 Si, with the remainder being Fe. The composition of the stainless steel 316L samples (by % weight) were 0.08 C, 2.00 Mn, 0.045 P, 0.030 S, 0.75 Si, 18.0 Cr, 10.0 Ni, 3.00 Mo, 0.10 N, and the remainder Fe. All working electrodes were sealed within multiple layers of polyolefin heat shrink tubing to expose a single-flat face with surface areas of 0.385 cm² and 0.2826 cm² for carbon steel and stainless steel, respectively.

2.3 Experimental Conditions

All solutions were made using ultrapure water with a conductivity of $18.2~M\Omega$ -cm obtained from a Milli-Q Millipore system. All experiments were performed at pH 10.6 in 0.01 M borate (Na₂B₄O₇) buffer solutions at room temperature, since the coolant in CANDU HTS is maintained at ~10.6, where the amount of soluble iron products is minimized. A pH of 10.6 was obtained by adding an appropriate amount of 1 M NaOH solution to the borate solution. Argon gas purging for one hour was used to eliminate dissolved oxygen before beginning each experiment. Hydrogen peroxide solutions were prepared from a 30% wt. stock solution.

The electrode system was irradiated in an MDS Nordian Gammacell 220 Excel, which has 60 Co pencils for the radiation source, having a half-life of 5.3 years. 60 Co emits γ -rays at energies of 1.17 and 1.33 MeV and emits β -particles with an energy of 318 keV (but these are blocked) [5]. The absorbed dose rate during the time in which the experiments were performed was measured by Fricke dosimetry to be 7.7 kGy/h.

All corrosion potential measurements were performed using an 8 channel Solartron 1480 potentiostat. CorrwareTM and Corrview software (supplied by Scribner and Associates) was used to control experiments and analyze data. The frequency analyzer used for Electrochemical Impedance Spectroscopy (EIS) measurements and analyses was a Solartron Frequency Response Analyzer 1255B. The frequency range in all EIS measurements was 10⁻² to 10⁴ Hz.

2.4 Experimental Procedure

The general experimental procedure is shown graphically in Figure 3.

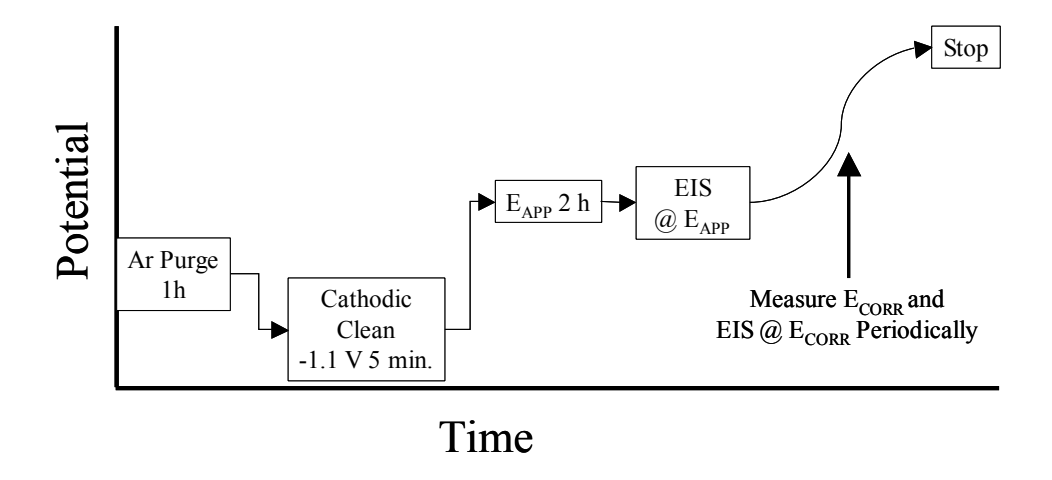


Figure 3: Experimental Procedure for Determining the Effects of Irradiation, or H₂O₂ Addition on Potentiostatically Grown Steel Oxide Films in 0.01 M Borate Solution at pH 10.6, 25°C.

All experiments began with polishing of the working electrodes on 400 grit followed by 600 grit polishing paper. The working electrodes were then rinsed with deionized water and placed in the electrochemical cell that had been purged with argon gas for 1 h to remove any oxygen in the solution. Electrochemical experiments then began with cathodic cleaning by applying a potential of -1.1 V (vs. SCE, or -1.0 vs. Hg/HgO) for 5 minutes to remove any air-formed oxides on the working electrode, thereby creating a clean metal surface. Various potentials were then applied for 2 hours (-0.8, -0.3, -0.2, and 0.2 V vs. SCE) to grow films with different compositions and properties. These potentials were chosen by reference to cyclic voltammetry experiments, which indicate the changes in behaviour of the steel at different potentials, see Figure 4 in Section 3. An EIS measurement was then performed at the applied potential to help characterize the oxide film that was grown. Measuring EIS at an applied potential, E_{APP} , implies the sinusoidal potential of \pm 10 mV was against E_{APP} and the current response was determined. Immediately following EIS at E_{APP} the cell was either lowered into the Gammacell to be exposed to radiation for 6 h, or H_2O_2 was added in varying

concentrations depending on the experiment being performed. During irradiation or H_2O_2 addition the corrosion potential, E_{CORR} , was measured as a function of time. E_{CORR} was measured for the 15 h following H_2O_2 addition, or the 6 h during irradiation and 12 h that followed the irradiation. Over the course of the E_{CORR} measurement EIS was performed periodically to help study the resistive and capacitive properties of the changing oxide film. To analyze the radiolytic production of redox species, the gas and aqueous samples were taken periodically for H_2O_2 analysis by UV-Vis Spectrophotometry and for O_2 and H_2 analysis by Gas Chromatography.

3. RESULTS AND DISCUSSION

3.1 Oxidation Regions of Carbon Steel and Stainless Steel

Before studying the effects of irradiation on steel and its various oxides, a better understanding of carbon steel and stainless steel oxides had to be established. To characterize the potential regions for anodic formation of oxide films, cyclic voltammograms were performed on both carbon steel and stainless steel in pH 10.6 borate solution. The cyclic voltammogram of carbon steel allows for the establishment of 3 general oxidation regions, Figure 4.

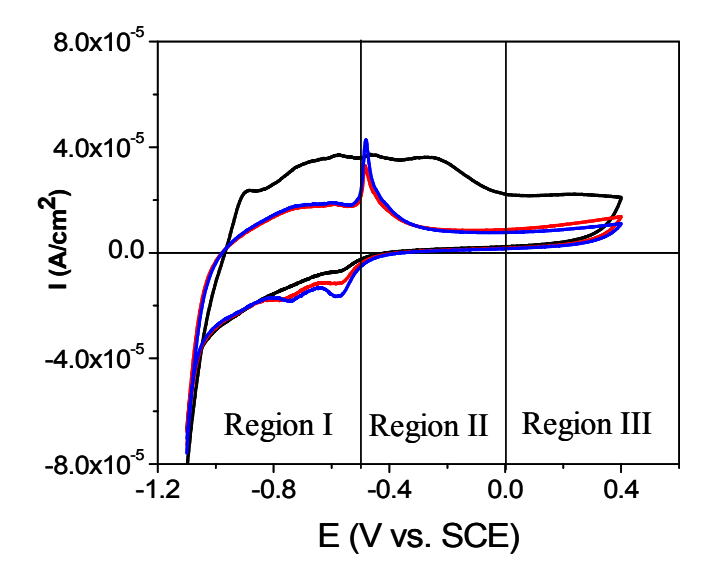


Figure 4: Cyclic Voltammogram of Carbon Steel in 0.01 M Borate Solution at pH 10.6, 25 °C. All Cycles Were Recorded Between Vertex Potentials of –1.1 V and 0.4 V vs. SCE at a Scan Rate of 5 mV/s.

A more detailed description of the oxidation regions of carbon steel can be found elsewhere [6]. As a brief description, Region I (-1.1 to -0.5 V) is composed of Fe(OH)₂ and some Fe₃O₄, Region II (-0.5 to 0 V) involves oxidation to Fe(III) oxides (Fe₂O₃ and FeOOH), and Region III (0 to 0.4 V) involves further oxidation to FeOOH accompanying some film restructuring.

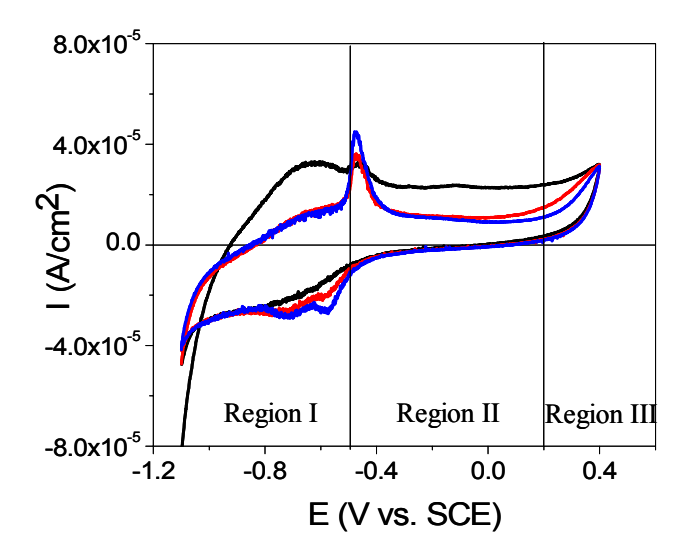


Figure 5: Cyclic Voltammogram of Stainless Steel 316L in 0.01 M Borate Solution at pH 10.6, 25°C. All Cycles Were Recorded Between Vertex Potentials of –1.1 V and 1.0 V vs. SCE at a Scan Rate of 50 mV/s.

The cyclic voltammogram performed on stainless steel 316L showed similar anodic current behaviour to the cyclic voltammogram of carbon steel. Some differences in the cyclic voltammogram arise from chromium oxides that formed or could have formed. At very low potentials, i.e., the beginning of Region I, chromium was oxidized to the Cr^{III} oxide Cr_2O_3 forming an initial passive layer [7]. The Cr_2O_3 passive layer was the reason why the current in Region I for stainless steel was slightly less than that seen for carbon steel. Also, at potentials in Region III chromium could have been further oxidized to the much more soluble Cr^{VI} species.

3.2 Potentiostatic Film Growth

Three different films were grown at -0.8 V (Region I), -0.2 V (Region II), or 0.2 V (Region III) for two hours before irradiation or H_2O_2 addition. The current-time (in $\log |i|$ vs. $\log t$ plots) and the charge (Q)-time behaviour observed during film growth are shown in Figure 6.

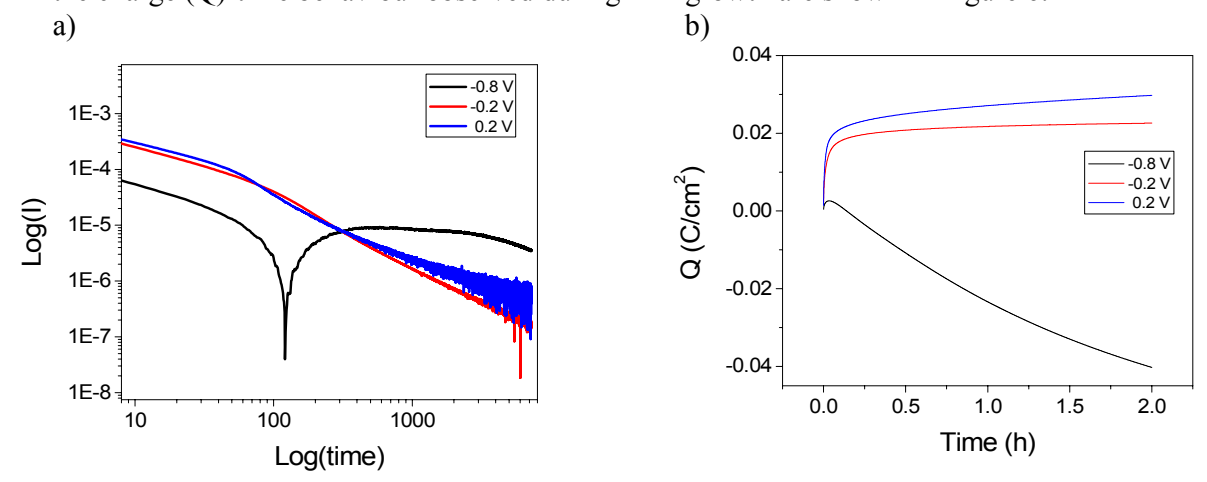


Figure 6: A Plot of a) Current-time and b) Charge-time Measured During Two Hours of Film Growth by Applying -0.8 V, -0.2 V, or 0.2 V With a Stainless Steel Working Electrode.

From these plots and our cyclic voltammograms we concluded that for the 2 h potentiostatic film growth the following oxides are present for stainless steel 316L:

$$\begin{array}{l} \text{At } E_{app} = \text{-0.8 V, } Cr_2O_3/Fe_3O_4 \\ \text{At } E_{app} = \text{-0.2 V, } Cr_2O_3/(Fe_3O_4 + Fe_2O_3) \\ \text{At } E_{app} = \text{ 0.2 V, } (Cr_2O_3 + Cr^{VI}) / (Fe_3O_4 + Fe_2O_3) \end{array}$$

For carbon steel, the iron oxides were the same for all E_{APP} , but obviously no chromium oxides were present. At this point, it has not been determined if the iron oxides are formed on top of the chromium oxide layer or they form different islands.

3.3 Analysis of Radiolysis Products

Spectrophotometric and Gas Chromatography measurements were taken periodically throughout the initial irradiation experiments to determine at what concentrations various redox species were produced.

Table 1: Concentrations of measured redox species formed under irradiation as function of irradiation time.

Time (h)	$H_2O_2(M)$	O ₂ (%)	H ₂ (%)
2	5.2×10^{-5}	0.8	0.5
4	8.0×10^{-5}	1.1	1.4
6	9.7 x 10 ⁻⁵	1.2	2.1

By analyzing the production of radiolytic redox species, we were able to perform bench top experiments outside of the gammacell to mimic irradiation conditions by adding redox species at concentrations equal to those produced under irradiation.

3.4 Corrosion Potential, E_{CORR}

The corrosion of metal can be considered of consisting of two half reactions, oxidation of metal species coupled with the reduction of aqueous species. The system consisting of the two half reactions soon achieves a steady-state potential. This potential defined as the corrosion potential (ECORR), sometimes referred to as the open circuit potential, or electrochemical corrosion potential (ECP), is the potential at which the system achieves charge balance. Due to the charge balance, the currents of the net anodic and net cathodic reactions at E_{CORR} must be opposite in sign but equal in magnitude. These currents at E_{CORR} are referred to as the corrosion current, i_{CORR} (i.e., $|\Sigma i_a| = |\Sigma i_c| = i_{CORR}$). Since this current is a measure of the rate of a reaction, the steel degradation can be determined if i_{CORR} can be measured. However, due to mass and charge balance, electrons are contained within a short circuit, resulting in zero net current, and the corrosion current cannot be measured directly. Nevertheless, the corrosion current as a function of E_{CORR} can be independently established using electrochemical analysis techniques. If this current-potential relationship is established and the E_{CORR} values achieved can be estimated, the corrosion rate of a given system can be determined.

Our main experiments involved measuring the corrosion potential, E_{CORR} , as a function of irradiation time and hydrogen peroxide concentration to follow the corrosion behaviour of steel. Specifically for both carbon steel and stainless steel 316L we measured the corrosion potential in a borate buffer solution during and after 6 h of irradiation, after the addition of 1 x 10^{-4} M H_2O_2 and

during the addition of H_2O_2 in 3 steps equal to concentrations produced under irradiation to better mimic irradiation conditions. To study the effects of these corrosive environments on the varying oxides of carbon steel and stainless steel we applied potentials of -0.8, -0.2, and 0.2 V vs. SCE for 2 h before irradiation or H_2O_2 addition. Those three potentials were chosen so we could study oxides across the three regions of oxidation that had been determined from the cyclic voltammogram.

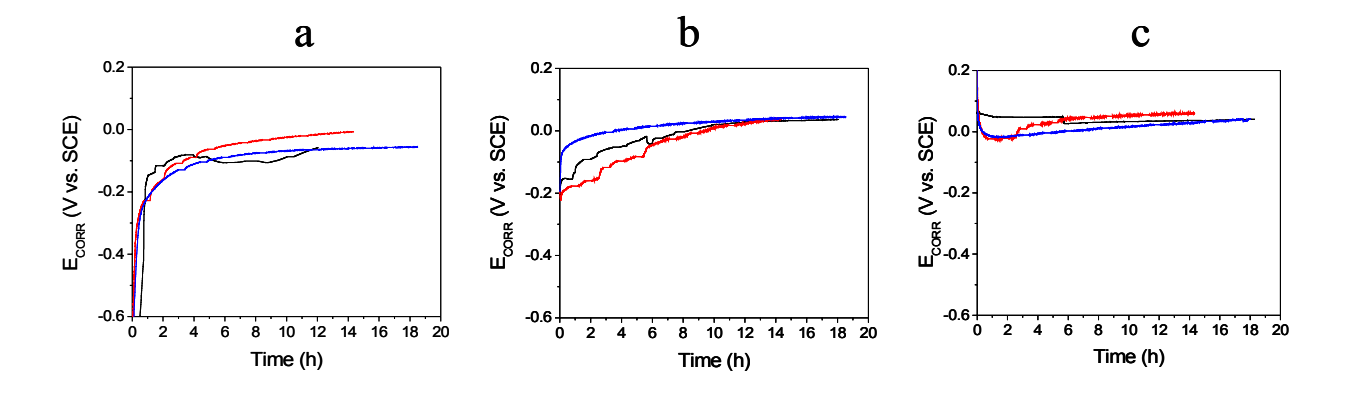


Figure 7: The Corrosion Potential Measured for Stainless Steel After the Application of a) -0.8 V, b) -0.2 V, and c) 0.2 V. The Black Line Represents the Case of 6 h Irradiation, the Red Line 4 x 10⁻⁵ M H₂O₂ Multi-step Addition at Times 0, 2, and 4 h, and the Blue Line 10⁻³ M H₂O₂ Single-step Addition.

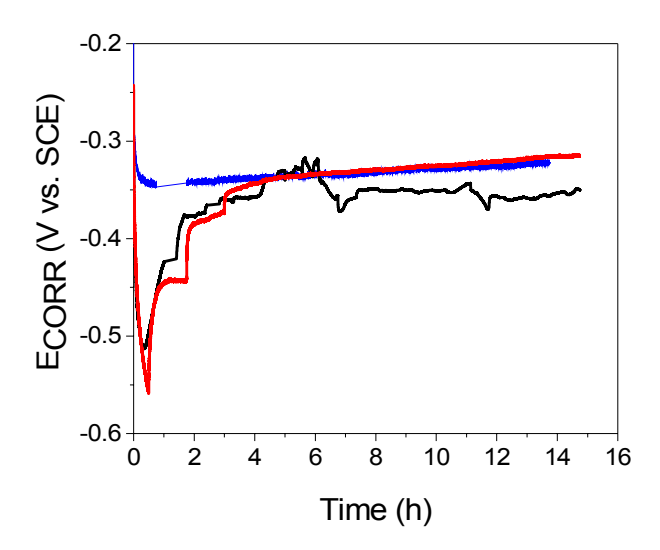


Figure 8: The Corrosion Potential Measured for Carbon Steel After Film Growth at -0.2 V. The Black Line Represents the Case of 6 h Irradiation, the Red Line 4 x 10⁻⁵ M H₂O₂ Multi-step Addition at Times 0, 2, and 4 h, and the Blue Line 10⁻⁴ M H₂O₂ Single-step Addition.

First, we found that E_{CORR} with the addition of H_2O_2 matched the changed in E_{CORR} under irradiation, especially when H_2O_2 was added in multiple steps. This shows the significance of H_2O_2 as most likely the key radiolytic redox species and shows the ability to simulate some irradiation experiments outside of the gammacell. For all cases, oxide films grown in Region I and II had an

increase in E_{CORR} upon addition of H_2O_2 or initiation of irradiation, while films grown in Region III had an initial decrease in E_{CORR} . Also, the rate of change of E_{CORR} for films grown in Region I were much higher and in all cases the rate of change of E_{CORR} lowered as irradiation time or time after H_2O_2 addition progressed. Upon completion of irradiation, or a few hours after H_2O_2 addition, both stainless steel and carbon steel reached a steady state E_{CORR} , with those values roughly being 0 V for stainless steel and -0.35 V for carbon steel.

Although EIS measurements were performed during the measurements of E_{CORR} , the results have yet to be completely summarized and therefore are not presented in this paper. Some early analysis has shown evidence of and increase in resistance and decrease in capacitance of the inner passive layer for stainless steel, signifying a thickening of the passive oxide layer. Further analysis will hopefully paint a better picture of the changing oxide layers.

4. CONCLUSIONS

In general, the oxidation behaviour of both carbon steel and stainless steel can be grouped into three different potential regions. Potentials from the three regions were applied to electrochemically grow different initial oxide films prior to irradiation. The rate of change in corrosion potential under irradiation was dependant on the initial film grown, however, for films grown in all three regions the corrosion potential reached similar steady state values of -0.35 V for carbon steel and 0 V for stainless steel. Also, the corrosion potential measurements could be reproduced with H_2O_2 addition, showing the importance of H_2O_2 as the key radiolytic redox species at room temperature. For H_2O_2 addition the change in corrosion potential was matched much closer when H_2O_2 was added in multiple steps instead of single steps because H_2O_2 was gradually being produced under irradiation. Finally, EIS measurements have not been completely analyzed, but initial results show a thickening of the passive layer, which coincides with the increasing corrosion potential for both carbon steel and stainless steel.

ACKNOWLEDGEMENT:

This research was funded under the Natural Science and Engineering Council of Canada (NSERC) and Atomic Energy of Canada Limited (AECL) Industrial Research Chair Agreement. The electrochemical analysis equipment was purchased by a grant from the Canada Foundation for Innovation.

5. REFERENCES

- 1. O.A. Olsson, D. Landolt, Passive films on stainless steels-chemistry, structure and growth, Electrochemica Acta 48 (2003) 1093-1104.
- 2. J.W.T. Spinks and R.J. Woods, Wiley-Interscience; 3 Sub edition, 243 (1990).
- 3. K. Ishigure, T. Nukii and S. Ono, Journal of Nuclear Materials, 350(1), 56 (2006).
- 4. C.C.Lin, Y.J. Kim, L.W. Niedrach, K.S. Ramp, CORROSION 52 (8), 618(1996)
- 5. Radioactive material data sheet. 2007 March. [cited March 12, 2007]. Available from: http://www.stuarthunt.com/Downloads/RMSDS/Co60.pdf
- 6. X. Zhang, W. Xu, D.W. Shoesmith, J.C. Wren, Kinetics of H₂O₂ reaction with oxide films on carbon steel, Corrosion Science 49 (2007) 4553-4567.
- 7. T. L. Wijensinghe, Investigating the Nature of Passive Films on Austenitic Stainless Steel, National University of Singapore (2005).